

Communication

# Generation of Vector Vortex Beams Based on the Optical Integration of Dynamic Phase and Geometric Phase

Kuiming Zeng<sup>1</sup>, Shanshan He<sup>1</sup>, Xianping Wang<sup>2,\*</sup> and Hailu Luo<sup>1,\*</sup> <sup>1</sup> Laboratory for Spin Photonics, School of Physics and Electronics, Hunan University, Changsha 410082, China<sup>2</sup> Jiangxi Key Laboratory of Photoelectronics and Telecommunication, College of Physics and Communication Electronics, Jiangxi Normal University, Nanchang 330022, China

\* Correspondence: xpwang@jxnu.edu.cn (X.W.); hailuluo@hnu.edu.cn (H.L.)

**Abstract:** The phase and polarization of electromagnetic waves can be conveniently manipulated by the dynamic phase and geometric phase elements. Here, we propose a compact optical integration of dynamic phase and geometric phase to generate arbitrary vector vortex beams on a hybrid-order Poincaré sphere. Two different technologies have been applied to integrate dynamic and geometric phase elements into a single glass plate to modulate the phase and polarization of light simultaneously. A spiral phase structure is made on one side of a glass substrate with optical lithography and a geometric phase metasurface structure is designed on the other side by femtosecond laser writing. The vector polarization is realized by the metasurface structure, while the vortex phase is generated by the spiral phase plate. Therefore, any desirable vector vortex beams on the hybrid-order Poincaré sphere can be generated. We believe that our scheme may have potential applications in future integrated optical devices for the generation of vector vortex beams due to its the high transmission efficiency and conversion efficiency.

**Keywords:** vortex beam; vector beam; metasurface; hybrid-order Poincaré sphere



**Citation:** Zeng, K.; He, S.; Wang, X.; Luo, H. Generation of Vector Vortex Beams Based on the Optical Integration of Dynamic Phase and Geometric Phase. *Photonics* **2023**, *10*, 214. <https://doi.org/10.3390/photronics10020214>

Received: 25 December 2022

Revised: 12 February 2023

Accepted: 13 February 2023

Published: 15 February 2023



**Copyright:** © 2023 by the authors. Licensee MDPI, Basel, Switzerland. This article is an open access article distributed under the terms and conditions of the Creative Commons Attribution (CC BY) license (<https://creativecommons.org/licenses/by/4.0/>).

## 1. Introduction

Phase and polarization are two important characteristics of electromagnetic waves and can be conveniently manipulated by the dynamic and geometric phase elements, respectively [1]. In general, the dynamic phase relates to the change in the optical path. To achieve the desired optical path difference, the space-variant profile or refractive index can be employed. In contrast, the Pancharatnam–Berry geometric phase results from the space-variant polarization. This approach for optical wave-front shaping is purely geometric in nature, and thus the related device is referred to as the geometric phase element [2]. There are different schemes based on the pure dynamic phase element or pure geometric phase one in the regulation of light [3–7]. Let us take the generation of vector vortex beams as an example. In the methods with pure dynamic phase devices, the modified interferometers may be employed [8–12]. In the methods with pure geometric phase elements, diversified schemes usually focus on several special cases, such as azimuthal and radial polarizations [13–24]. Vector vortex beams have found a wide range of applications including microscopy [25], optical trapping [26], metrology [27], and quantum communication [28]. In some applications of classic and quantum regimes, a compact optical element for flexible modulation of vector vortex states of photons is needed.

In this paper, we propose to integrate a metasurface  $q$ -plate and a spiral phase plate into a single glass plate to generate arbitrary vector vortex beams. Figure 1a,b show schematic diagrams of the  $q$ -plate and the spiral phase plate, respectively. In our scheme, a homogeneous polarized Gaussian beam is converted into a vector beam by a metasurface  $q$ -plate. After passing through the spiral phase plate, the vector beam is further converted into a vector vortex beam. Therefore, we can integrate the metasurface  $q$ -plate and the spiral

phase plate into a single glass plate to construct a compact optical element for the flexible generation of vector vortex beams. The schematic photograph of the glass vector-vortex plate and is plotted in Figure 1c. The SEM image of the metasurface  $q$ -plate structure is shown in Figure 1d. The local optical directions of fast and slow axes are perpendicular and parallel to the grooves, respectively. The fabricated metasurface structure can be regarded as a birefringent waveplate with homogeneous phase retardation and a locally varying optical axis direction, since the characteristic dimension of the nanostructure is much smaller than the operational wavelength. The metasurface  $q$ -plate can be constructed by controlling the orientation of the nano grooves. In fact, the glass vector vortex plate is a combination of the geometric phase  $q$ -plate that is designed by femtosecond laser writing and the spiral phase plate which is made with optical lithography. Compared with other complex devices to regulate geometric and dynamic phases, this integrated glass plate has compact advantages and convenient operation.

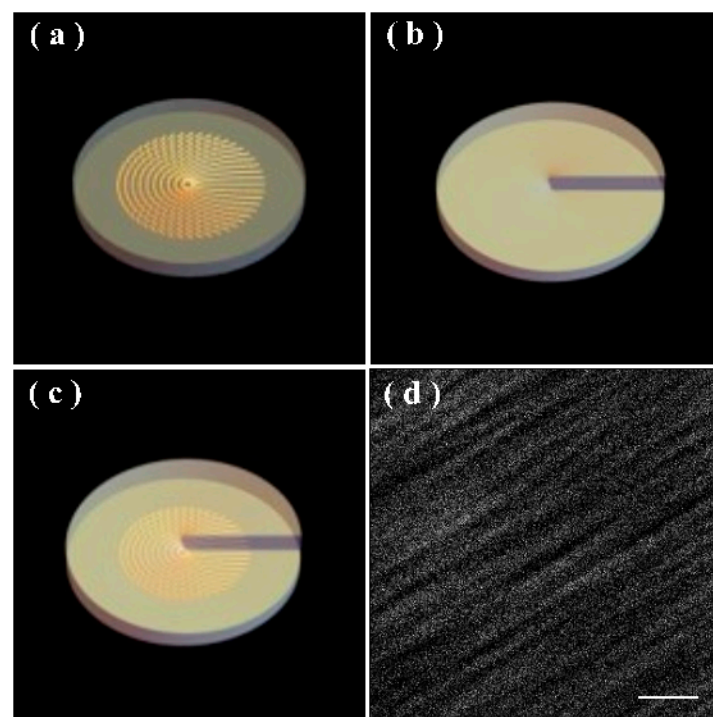


**Figure 1.** Schematic illustration of (a) the metasurface  $q$ -plate, (b) the spiral phase plate, and (c) the integrated glass vector-vortex plate. (d) The SEM image of the designed metasurface nanostructures, scale bar, 200 nm.

## 2. Optical Integration of Dynamic Phase and Geometric Phase

It is known that the states of vector vortex beams can be described by the hybrid-order Poincaré sphere [29–35]. All points on the surface of Poincaré sphere can be represented as a superposition of these two orthogonal circular polarizations with different topological charges. In the paraxial approximation, a generalized vector vortex state can be represented as a superposition of these two orthogonal circular polarization states with different topological charges in the following formular:

$$|\Psi\rangle = \Psi_N^l |\mathbf{R}\rangle \exp \frac{i l \varphi}{2} + \Psi_S^m |\mathbf{L}\rangle \exp \frac{i m \varphi}{2} \quad (1)$$

Here,  $|\mathbf{R}\rangle = (e_x + i e_y) / \sqrt{2}$  and  $|\mathbf{L}\rangle = (e_x - i e_y) / \sqrt{2}$ ,  $e_x$  and  $e_y$  are separately the unit vectors along the  $x$  and  $y$  axes in the Cartesian coordinate system. Any polarization state  $(\theta, \varphi)$  on hybrid-order Poincaré can be described as a superposition of the orthogonal bases with coefficients  $\Psi_N^l$  and  $\Psi_S^m$ , respectively. Figure 2 depicts a hybrid-order Poincaré

sphere with  $l = 0$  and  $m = +2$ . Here,  $l$  and  $m$  are the topological charges, which is related to orbital angular momentum of light [36].

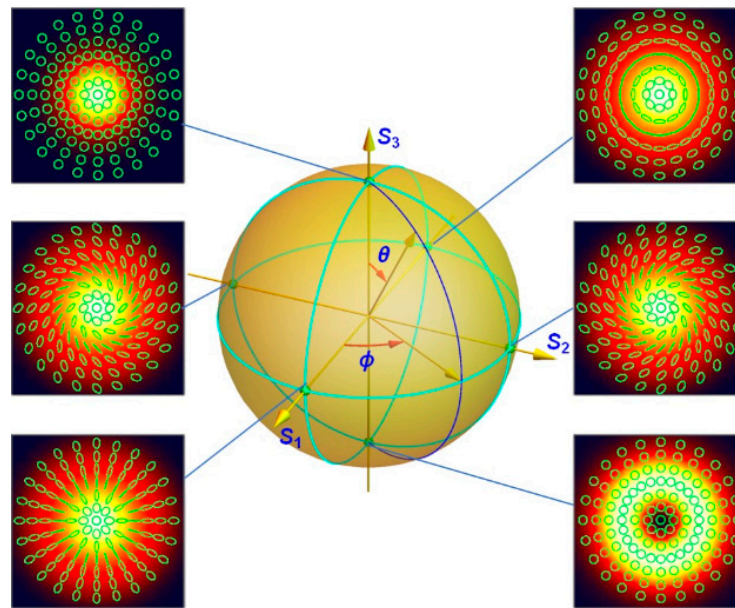


**Figure 2.** Schematic illustration of the hybrid-order Poincaré sphere with  $l = 0$  and  $m = 2$ . The polarization and intensity distribution of vector vortex beams corresponding to four points on the equator and two poles.

After extracting a vortex phase factor  $\exp[i(l + m)\phi/2]$ , Equation (1) can be written as [37].

$$|\Psi\rangle = \exp\frac{i(l + m)\phi}{2} \left[ \Psi_N^l |\mathbf{R}\rangle \exp\frac{i(l - m)\phi}{2} + \Psi_S^m |\mathbf{L}\rangle \exp\frac{i(m - l)\phi}{2} \right] \quad (2)$$

Comparing Equation (1) with Equation (2) shows that the vector vortex states can be divided into a vortex phase and a vector polarization. In general, the vortex phase can be generated with spiral phase plate and the vector polarization can be generated with  $q$ -plate. To construct a compact optical element, we therefore propose to fabricate a spiral phase structure on one side of the glass substrate with optical lithography and a geometric phase  $q$ -plate on the other side by femtosecond laser writing.

The optical lithography is chosen to fabricate the spiral phase plate on the one side of the glass substrate [38]. It is known that the optical thickness of the spiral phase plate is proportional to the azimuthal angle. The fabrication details are as follows: Assuming that the diameter of the spiral phase plate is  $D$ , we quantize an irregular three-dimensional surface of a spiral phase plate into two dimensional bars to form a binary mask by selecting the suitable interval  $d$ . Then we obtain  $N = D/d$  micro-slices. Each different slice is projected and zoomed in the same scale to form the 2D binary sub-mask. By moving the mask at a certain speed in the exposure process, the distribution at each quantized unit is modulated by the corresponding sub-mask. The fabricated 3D structure is determined by the mask and the exposure dose. The thickness of optical lithography increases as the exposure dose.

The fabrication three-dimensional surface structure with a phase retardation value ranging from 0 to  $2\pi$  at a wavelength of 632.8 nm is acquired. In our case, the thickness of the glass substrate is 3 mm with the diameter  $D = 25.4$  mm. Take the spiral phase plate used for  $l = 1$ , and the phase modulation is  $2\pi$ ; the step height can be obtained by  $h = \lambda/(n - 1)$ , where  $n = 1.458$  is the refractive index of silica. Therefore, the theoretical step height is obtained as  $h = 1.381 \mu\text{m}$ . After exposure and optical lithography, the step

height of spiral surface is obtained by optical surface profile as 1.385  $\mu\text{m}$ , which coincides well with the theoretical value.

Figure 3a shows the measured phase retardation value distribution of the spiral phase plate ( $l = 1$ ). To ensure the phase structure of the output beams, the interference patterns are measured with the Mach–Zehnder interferometer which is similar to the experimental setup in Ref. [39]. In our experiment, the interference patterns of the generated vortex beam with a plane wave and a spherical wave are measured, respectively Figure 3b,c.

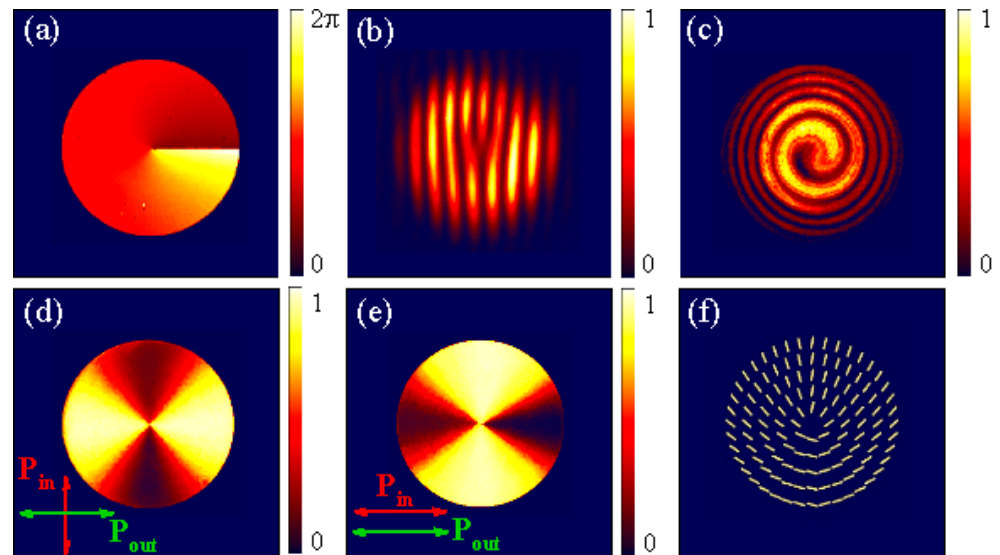


**Figure 3.** (a) Experimentally measured phase retardation of spiral phase structure ( $l = 1$ ). (b,c) are the measured intensity patterns of the generated vortex beam interfering with a plane wave and a spherical wave, respectively. (d,e) Polariscopic images of optical axis distribution of the glass vector-vortex plate under crossed polarizers.  $P_{in}$  and  $P_{out}$  stand for the polarization states of the input and output beams, respectively. (f) The optical axis distribution of the q plate is retrieved by the polariscopic images.

The metasurface  $q$ -plate structure is designed on the other side of glass plate by means of a femtosecond laser engraving space-variant nanogrooves. The written area is centered on the glass plate. Under the laser irradiation, the fused glass ( $\text{SiO}_2$ ) decomposes into porous glass ( $\text{SiO}_2 + \text{O}_2$ ), whose refractive index is controlled by the laser intensity. The filling factor is 0.1–0.2, the line width is 30–50 nm, and the depth of nanogrooves is approximately equal to 80 nm. The measured diffraction and transmission efficiency for the nanostructures are 89.4% and 58.7% at the wavelength of 632.8 nm, respectively. Because the characteristic dimension of the structure is much smaller than the operational wavelength, the nanostructure can be regarded as a birefringent waveplate with homogeneous phase retardation and a locally varying optical axis direction. The phase retardation is  $\varphi = (n_e - n_o)h/\lambda$ , where  $h$  is the writing depth and  $n_e - n_o$  is the induced birefringence. As a linear approximation, the effective ordinary and extraordinary refractive indices can be written as [40].

$$n_o = \sqrt{fn_1^2 + (1 - f)n_2^2}, \quad n_e = \sqrt{\frac{n_1^2 n_2^2}{(1 - f)n_1^2 + fn_2^2}} \quad (3)$$

Here,  $f$  is the filling factor, and  $n_1$  and  $n_2$  are the refractive indices of the two media that form the grating-like structure. The birefringence value of  $n_e - n_o$  is about  $-3 \times 10^{-3}$ , and the retardation is  $\varphi = \pi$ . Note that this technology has been extensively applied to fabricate spin-based photonics devices, such as vector beam generator [41], spin-dependent beam splitter [42], spin-Hall metalens [43], and optical spatial differentiator [44–48].

The metasurface  $q$ -plate with a uniform birefringent phase retardation  $\pi$  at a wavelength of 632.8 nm acts as a half wave plate with inhomogeneous distribution of optical axis. Its optical axis distribution satisfies  $\Psi = q\phi + \Psi_0$ , where  $q$  is the spatial rotational rate of the optical axis,  $\phi$  is the azimuth angle, and  $\Psi_0$  is the initial angle. Here, by etching space-variant grooves on a fused silica sample using a femtosecond laser, we need to fabricate the  $q$ -plate ( $q = 1/2$ ) with a diameter of 4 mm at the flat surface of the spiral phase plate ( $l' = 1$ ), the diameter of which is 25.4 mm, and keep the center of the  $q$ -plate and the spiral phase plate aligned. The optical axis distribution of the  $q$ -plate on the integrated vector-vortex plate can be retrieved by two crossed polarizers. Because the spiral structure of the integrated plate does not affect the polarization state of the beams, we obtain the cross polarized images of  $q$ -plate under cross and line polarizers, respectively, as shown in Figure 3d,e. The orientation of optical axis of the  $q$ -plate is shown in Figure 3f which is retrieved from Figure 3d based on the optical Malus law [1].

### 3. Generation of Vector Vortex Beams

In our experiment, the integrated glass vector-vortex plate (VVP) with  $q = 1/2$  and  $l' = 1$  was used to verify the generation of arbitrary vector vortex beams on the hybrid-order Poincaré sphere. As shown in Figure 4, a Glan laser polarizer (GLP1) and a quarter-wave plate (QWP1) convert the laser beam from the He-Ne laser (632.8 nm, 21 mW) into a homogenous elliptical polarization. The polarization of input beam can be modulated by GLP1 and QWP1 which can realize any desired polarization states on the fundamental Poincaré sphere. The azimuth angle  $\eta$  of the output polarization state is equal to the angle between the optical axis direction of QWP1 and the vertical direction. The elliptical angle  $\delta$  is equal to the relative angle of the optical axis direction between GLP1 and QWP1. A relationship between  $(\eta, \delta)$  and vector vortex states on the hybrid-order Poincaré sphere  $(\theta, \phi)$  can be established  $\eta = \phi$  and  $\delta = (2\theta - \pi)/4$  [40]. The incident beam first passes through the plane of the  $q$ -plate and then through the spiral phase surface, resulting in the transformation of a fundamental Gaussian beam into a vector vortex beam. A typical setup (QWP2, GLP2, and CCD) measures the Stokes parameters that describe the polarization state and intensity of the output light. The polarization distribution of the generated vector vortex beams can be effectively retrieved by the measurement of Stokes parameters [34].

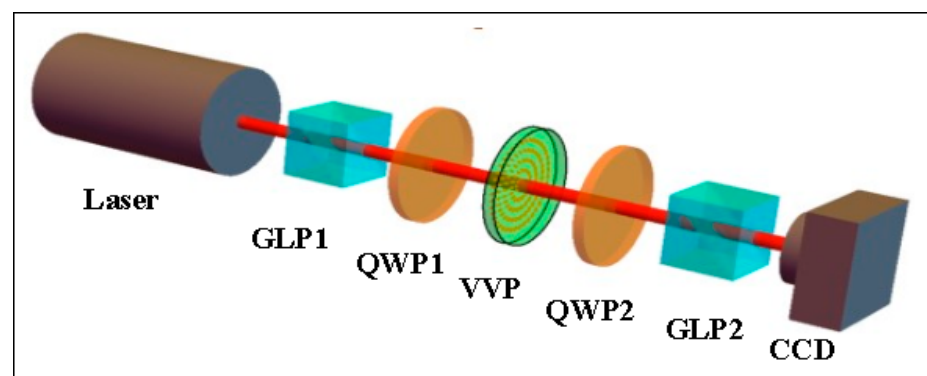


**Figure 4.** Experimental setup to generate arbitrary vector vortex beams on the hybrid-order Poincaré sphere. GLP, Glan laser polarizer; QWP, quarter-wave plate; VVP, vector-vortex plate; CCD, charge-coupled device.

To evaluate the quality of the generated vector vortex beams, we measure the polarization and phase distributions of the resultant vector vortex beams. After the polarization state is obtained, we remove the QWP2 in the experimental device and adjust the optical axis of GLP2 to the vertical state (the rotation angle of the optical axis is 0). The CCD records the intensity distributions of the generated vector vortex beams to determine the vortex phase for linear and elliptical polarization beams. When the circular polarization beams of two poles are produced, the topological charge can be determined by the Mach–Zehnder

interferometer, which is similar to the experimental setup in Ref. [32]. The topological charges of the output beams from the glass vector-vortex plate are thus equal to  $(-2q + l)$  and  $(+2q + l')$ , which are, respectively, 0 and 2 in our scheme.

Figure 5 shows theoretical and experimental distributions of polarization states and phase for four points on the equator of the hybrid-order Poincaré sphere. The theoretic results of intensity and polarization distribution are plotted in Figure 5a–d. The polarization states on the cross section of the emerging beams can effectively retrieved by measuring the Stokes parameters (Figure 5e–h). After removing the QWP2, the theoretic results reflecting the vortex phase structure are plotted in Figure 5i–l. The experimental patterns are recorded by the CCD (Figure 5m–p). Four typical s-shaped patterns which show double charged optical vortices exhibit different directions which are determined by the polarization pattern of the emergent beams. These s-shaped light intensity images indicate that the topological charge of the generated beams is 1. It is shown that linear polarization direction of points on the equator are composed of equal superposition of a fundamental-mode Gaussian beam and a Laguerre–Gaussian beam.

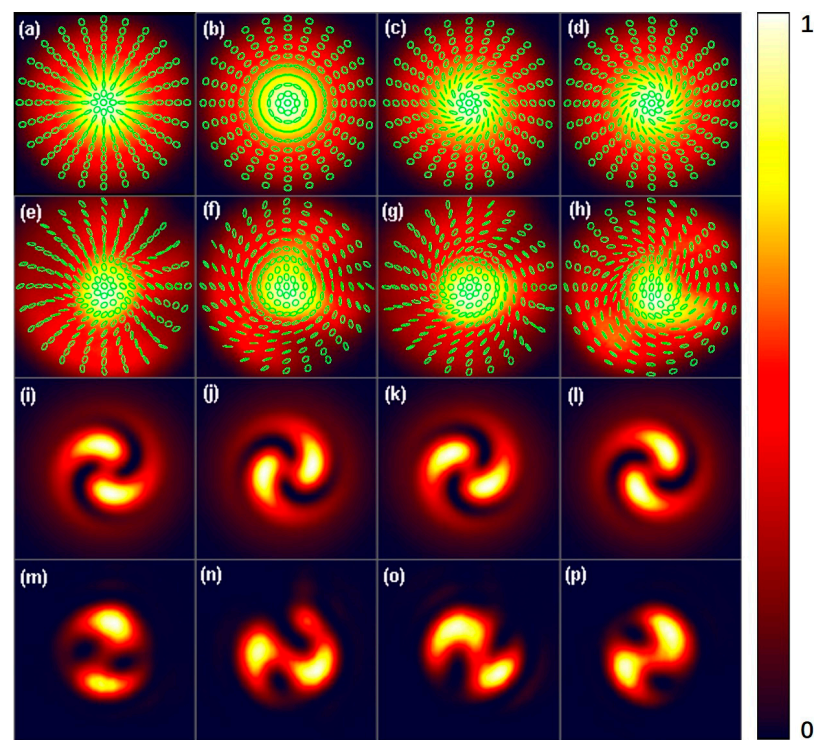


**Figure 5.** Polarization and intensity distributions of the generated vector vortex beams. (a–d) The theoretic polarization and intensity distributions for the points  $(1,0,0)$ ,  $(-1,0,0)$ ,  $(0,1,0)$ , and  $(0,-1,0)$  on the hybrid-order Poincaré sphere in the order from left to right. (e–h) The corresponding experimental results. (i–l) The theoretic intensity distributions of the linearly polarized vortex beams after passing a horizontal polarizer. (m–p) The corresponding experimental results.

It should be noted that the diffraction will lead to the inconsistency of bright spots shown in the third and fourth row and the results shown in the first two rows in Figure 5. The intensity distribution in the third and fourth row can be regarded as the interference of fundamental Gaussian beam, a vortex beam with  $l = 1$ . It is known that the rotation effect presents during propagation, where the rotation angle is proportion to the Gouy phase shift. Note that the analytical forms for vector vortex beams can be obtained in the Fresnel and Fraunhofer diffraction regions based on a strict prorogation model [49,50].

Comparing with Figure 5, the vector vortex beams on two poles and two ordinary points on the hybrid-order Poincaré sphere are shown in Figure 6. The theoretic results of intensity and polarization distribution are plotted in Figure 6a–d. The polarization states

on the cross section of the emerging beams can be effectively retrieved by measuring the Stokes parameters (Figure 6e–h). The theoretic results proving phase distribution of the generated vector vortex beams are shown in Figure 6i–l. For the circular polarization beams, the interference patterns of the output beams and the reference Gaussian beam demonstrate that north and south poles represent a fundamental-mode Gaussian beam and a Laguerre–Gaussian beam, respectively (Figure 6m,n). The fork-like patterns give expression to the vortex phase with different topological charges. For elliptical polarization beams on two ordinary points, the CCD records two typical s-shaped patterns after removing the QWP2 (Figure 6o,p). The major reason for the slight deformation in intensity distribution of the generated vector vortex beams is attributed to the inaccuracy in writing the center of q-plate. Due to the errors caused by the integrated manufacturing process, the center of the q-plate cannot be strictly aligned with the center of the spiral phase plate, resulting in slight distortion of the light spot. In addition, the polarization error of the generated vector vortex beam is due to the difficulty in guaranteeing that the pictures of Stokes parameters are the same pixels.

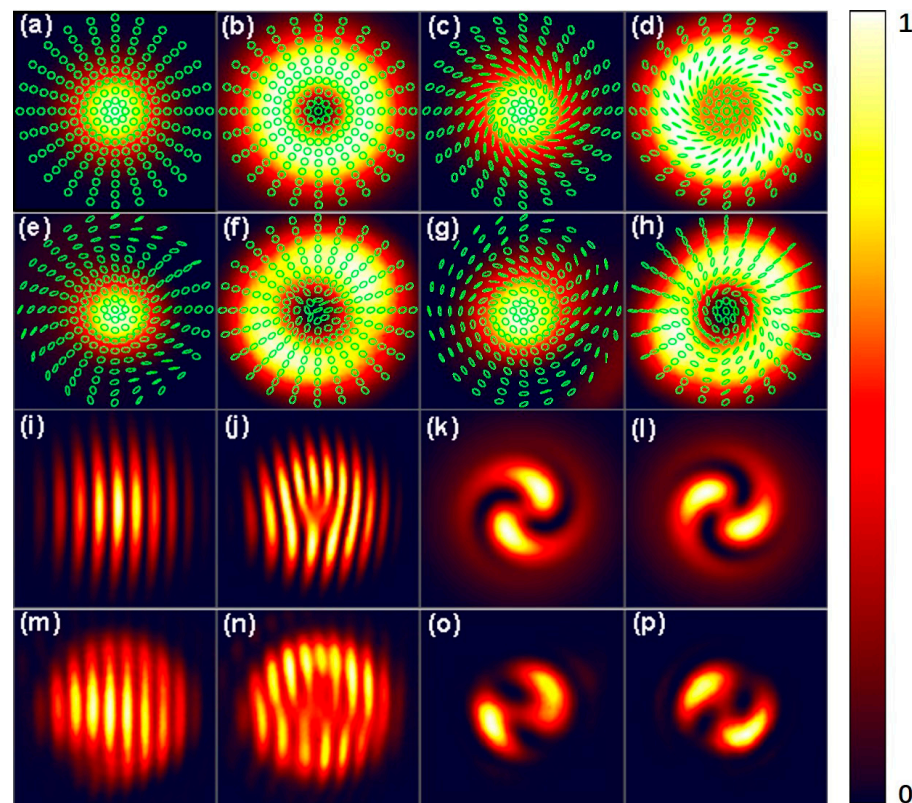


**Figure 6.** Polarization and intensity distributions of the generated vector vortex beams. (a–d) The theoretical polarization and intensity distributions for the points  $(0, 0, 1)$ ,  $(0, 0, -1)$ ,  $(0, -\sqrt{2}/2, \sqrt{2}/2)$ , and  $(0, \sqrt{2}/2, -\sqrt{2}/2)$  on the hybrid-order Poincaré sphere in order from left to right. (e–h) The corresponding experimental results. (i–l) The theoretical interference patterns of two poles and intensity distributions of the elliptically polarized vortex beams behind a horizontal polarizer. (m–p) The corresponding experimental results.

#### 4. Conclusions

We have proposed a compact optical integration of dynamic phase and geometric phase to generate arbitrary vector vortex beams on a hybrid-order Poincaré sphere. The glass vector-vortex plate with integrated a metasurface q-plate and a spiral phase plate has been proposed and experimentally demonstrated. By tuning the incident polarization states, any desired vector vortex beams on the hybrid-order Poincaré sphere can be realized. The integrated glass vector vortex plate provides a possible way to generate vector vortex

beams in a flexible and highly efficient way. More importantly, our results provide an approach to controlling the dynamic phase and geometric phase simultaneously, thereby enabling a compact optical element in the flexible generation of vector vortex beams.

**Author Contributions:** Conceptualization, H.L.; methodology, K.Z. and S.H.; writing—original draft preparation, K.Z. and S.H.; writing—review and editing, K.Z., X.W. and H.L.; supervision, X.W. and H.L. All authors have read and agreed to the published version of the manuscript.

**Funding:** This research was funded in part by the National Natural Science Foundation of China (No. 12064017).

**Institutional Review Board Statement:** Not applicable.

**Informed Consent Statement:** Informed consent was obtained from all subjects involved in the study.

**Data Availability Statement:** Not applicable.

**Conflicts of Interest:** The authors declare no conflict of interest.

## References

1. Born, M.; Wolf, E. *Principles of Optics*, 7th ed.; Cambridge University Press: Cambridge, UK, 1999.
2. Hasman, E.; Biener, G.; Niv, A.; Kleiner, V. Space-variant polarization manipulation. *Prog. Opt.* **2005**, *47*, 215–289. [[CrossRef](#)]
3. Zhan, Q. Cylindrical vector beams: From mathematical concepts to applications. *Adv. Opt. Photonics* **2009**, *1*, 1–57. [[CrossRef](#)]
4. Li, P.; Zhang, Y.; Liu, S.; Ma, C.; Han, L.; Cheng, H.; Zhao, J. Generation of perfect vectorial vortex beams. *Opt. Lett.* **2016**, *41*, 2205–2208. [[CrossRef](#)] [[PubMed](#)]
5. Xu, D.; Gu, B.; Rui, G.; Zhan, Q.; Cui, Y. Generation of arbitrary vector fields based on a pair of orthogonal elliptically polarized base vectors. *Opt. Express* **2016**, *24*, 4177–4186. [[CrossRef](#)] [[PubMed](#)]
6. Fu, S.; Zhai, Y.; Wang, T.; Yin, C.; Gao, C. Tailoring arbitrary hybrid Poincaré beams through a single hologram. *Appl. Phys. Lett.* **2017**, *111*, 211101. [[CrossRef](#)]
7. Bai, Y.; Zhang, Q.; Yang, Y. Generation of Tunable Plasmonic Vortices by Varying Wavelength of Incident Light. *Photonics* **2022**, *9*, 809. [[CrossRef](#)]
8. Chen, H.; Hao, J.; Zhang, B.-F.; Xu, J.; Ding, J.; Wang, H.-T. Generation of vector beam with space-variant distribution of both polarization and phase. *Opt. Lett.* **2011**, *36*, 3179–3181. [[CrossRef](#)]
9. Galvez, E.J.; Khadka, S.; Schubert, W.H.; Nomoto, S. Poincaré-beam patterns produced by nonseparable superpositions of Laguerre–Gauss and polarization modes of light. *Appl. Opt.* **2012**, *51*, 2925–2934. [[CrossRef](#)]
10. Chen, S.; Zhou, X.; Liu, Y.; Ling, X.; Luo, H.; Wen, S. Generation of arbitrary cylindrical vector beams on the higher order Poincaré sphere. *Opt. Lett.* **2014**, *39*, 5274–5276. [[CrossRef](#)]
11. Chen, Z.; Zeng, T.; Qian, B.; Ding, J. Complete shaping of optical vector beams. *Opt. Express* **2015**, *23*, 17701–17710. [[CrossRef](#)]
12. Chen, Y.; Gu, J.; Wang, F.; Liu, L.; Zhao, C.; Cai, Y.; Korotkova, O. Generation and propagation of a partially coherent vector beam with special correlation functions. *Phys. Rev. A* **2014**, *89*, 013801. [[CrossRef](#)]
13. Stalder, M.; Schadt, M. Linearly polarized light with axial symmetry generated by liquid-crystal polarization converters. *Opt. Lett.* **1996**, *21*, 1948. [[CrossRef](#)] [[PubMed](#)]
14. Bomzon, Z.; Biener, G.; Kleiner, V.; Hasman, E. Radially and azimuthally polarized beams generated by space-variant dielectric subwavelength gratings. *Opt. Lett.* **2002**, *27*, 285–287. [[CrossRef](#)] [[PubMed](#)]
15. Marrucci, L.; Manzo, C.; Paparo, D. Optical Spin-to-Orbital Angular Momentum Conversion in Inhomogeneous Anisotropic Media. *Phys. Rev. Lett.* **2006**, *96*, 163905. [[CrossRef](#)]
16. Deng, D.; Guo, Q. Analytical vectorial structure of radially polarized light beams. *Opt. Lett.* **2007**, *32*, 2711. [[CrossRef](#)]
17. Beresna, M.; Gecevičius, M.; Kazansky, P.G.; Gertus, T. Radially polarized optical vortex converter created by femtosecond laser nanostructuring of glass. *Appl. Phys. Lett.* **2011**, *98*, 201101. [[CrossRef](#)]
18. Chen, P.; Ji, W.; Wei, B.-Y.; Hu, W.; Chigrinov, V.; Lu, Y.-Q. Generation of arbitrary vector beams with liquid crystal polarization converters and vector-photoaligned q-plates. *Appl. Phys. Lett.* **2015**, *107*, 241102. [[CrossRef](#)]
19. Naidoo, D.; Roux, F.S.; Dudley, A.; Litvin, I.; Piccirillo, B.; Marrucci, L.; Forbes, A. Controlled generation of higher-order Poincaré sphere beams from a laser. *Nat. Photonics* **2016**, *10*, 327–332. [[CrossRef](#)]
20. Sánchez-López, M.M.; Davis, J.A.; Hashimoto, N.; Moreno, I.; Hurtado, E.; Badham, K.; Tanabe, A.; Delaney, S.W. Performance of a q-plate tunable retarder in reflection for the switchable generation of both first- and second-order vector beams. *Opt. Lett.* **2016**, *41*, 13–16. [[CrossRef](#)]
21. Yue, F.; Wen, D.; Xin, J.; Gerardot, B.D.; Li, J.; Chen, X. Vector Vortex Beam Generation with a Single Plasmonic Metasurface. *ACS Photonics* **2016**, *3*, 1558–1563. [[CrossRef](#)]
22. Rafayelyan, M.; Gertus, T.; Brasselet, E. Laguerre-Gaussian quasi-modal q-plates from nanostructured glasses. *Appl. Phys. Lett.* **2017**, *110*, 261108. [[CrossRef](#)]



23. Song, R.; Liu, X.; Fu, S.; Gao, C. Simultaneous tailoring of longitudinal and transverse mode inside an Er: YAG laser. *Chin. Opt. Lett.* **2021**, *19*, 111404. [[CrossRef](#)]
24. Fu, S.; Hai, L.; Song, R.; Gao, C.; Zhang, X. Representation of total angular momentum states of beams through a four-parameter notation. *New J. Phys.* **2021**, *23*, 083015. [[CrossRef](#)]
25. Abouraddy, A.F.; Toussaint, K.C., Jr. Three-Dimensional Polarization Control in Microscopy. *Phys. Rev. Lett.* **2006**, *96*, 153901. [[CrossRef](#)] [[PubMed](#)]
26. Roxworthy, B.J.; Toussaint, K.C., Jr. Optical trapping with  $\pi$ -phase cylindrical vector beams. *New J. Phys.* **2010**, *12*, 073012. [[CrossRef](#)]
27. Wang, B.; Tanksalvala, M.; Zhang, Z.; Esashi, Y.; Jenkins, N.W.; Murnane, M.M.; Kapteyn, H.C.; Liao, C. Coherent Fourier scatterometry using orbital angular momentum beams for defect detection. *Opt. Express* **2021**, *29*, 3342–3358. [[CrossRef](#)]
28. Parigi, V.; D'Ambrosio, V.; Arnold, C.; Marrucci, L.; Sciarrino, F.; Laurat, J. Storage and retrieval of vector beams of light in a multiple-degree-of-freedom quantum memory. *Nat. Commun.* **2015**, *6*, 7706. [[CrossRef](#)]
29. Milione, G.; Sztul, H.I.; Nolan, D.A.; Alfano, R.R. Higher-order Poincaré sphere, Stokes parameters, and the angular momentum of light. *Phys. Rev. Lett.* **2011**, *107*, 053601. [[CrossRef](#)]
30. Holleczek, A.; Aiello, A.; Gabriel, C.; Marquardt, C.; Leuchs, G. Classical and quantum properties of cylindrically polarized states of light. *Opt. Express* **2011**, *19*, 9714–9736. [[CrossRef](#)]
31. Milione, G.; Evans, S.; Nolan, D.A.; Alfano, R.R. Higher Order Pancharatnam-Berry Phase and the Angular Momentum of Light. *Phys. Rev. Lett.* **2012**, *108*, 190401. [[CrossRef](#)]
32. Cardano, F.; Karimi, E.; Slussarenko, S.; Marrucci, L.; de Lisio, C.; Santamato, E. Polarization pattern of vector vortex beams generated by q-plates with different topological charges. *Appl. Opt.* **2012**, *51*, C1–C6. [[CrossRef](#)]
33. Yi, X.; Liu, Y.; Ling, X.; Zhou, X.; Ke, Y.; Luo, H.; Wen, S. Hybrid-order Poincaré sphere. *Phys. Rev. A* **2015**, *91*, 023801. [[CrossRef](#)]
34. Liu, Y.; Liu, Z.; Zhou, J.; Ling, X.; Shu, W.; Luo, H.; Wen, S. Measurements of Pancharatnam–Berry phase in mode transformations on hybrid-order Poincaré sphere. *Opt. Lett.* **2017**, *42*, 3447–3450. [[CrossRef](#)] [[PubMed](#)]
35. Wang, R.; He, S.; Chen, S.; Zhang, J.; Shu, W.; Luo, H.; Wen, S. Electrically driven generation of arbitrary vector vortex beams on the hybrid-order Poincaré sphere. *Opt. Lett.* **2018**, *43*, 3570–3573. [[CrossRef](#)] [[PubMed](#)]
36. Allen, L.; Beijersbergen, M.W.; Spreeuw, R.J.C.; Woerdman, J.P. Orbital angular momentum of light and the transformation of Laguerre-Gaussian laser modes. *Phys. Rev. A* **1992**, *45*, 8185–8189. [[CrossRef](#)] [[PubMed](#)]
37. Liu, Z.; Liu, Y.; Ke, Y.; Liu, Y.; Shu, W.; Luo, H.; Wen, S. Generation of arbitrary vector vortex beams on hybrid-order Poincaré sphere. *Photon. Res.* **2017**, *5*, 15–21. [[CrossRef](#)]
38. Shi, L.; Zhang, Z.; Cao, A.; Luo, X.; Deng, Q. One exposure processing to fabricate spiral phase plate with continuous surface. *Opt. Express* **2015**, *23*, 8620–8629. [[CrossRef](#)] [[PubMed](#)]
39. He, Y.; Liu, Z.; Liu, Y.; Zhou, J.; Ke, Y.; Luo, H.; Wen, S. Higher-order laser mode converters with dielectric metasurfaces. *Opt. Lett.* **2015**, *40*, 5506–5509. [[CrossRef](#)] [[PubMed](#)]
40. Beresna, M.; Gecevičius, M.; Kazansky, P. Polarization sensitive elements fabricated by femtosecond laser nanostructuring of glass. *Opt. Mater. Express* **2011**, *1*, 783–795. [[CrossRef](#)]
41. Liu, Y.; Ling, X.; Yi, X.; Zhou, X.; Luo, H.; Wen, S. Realization of polarization evolution on higher-order Poincaré sphere with metasurface. *Appl. Phys. Lett.* **2014**, *104*, 191110. [[CrossRef](#)]
42. Ling, X.; Zhou, X.; Yi, X.; Shu, W.; Liu, Y. Giant photonic spin Hall effect in momentum space in a structured metamaterial with spatially varying birefringence. *Light Sci. Appl.* **2015**, *4*, e290. [[CrossRef](#)]
43. Zhou, J.; Qian, H.; Hu, G.; Luo, H.; Wen, S.; Liu, Z. Broadband Photonic Spin Hall Meta-Lens. *ACS Nano* **2018**, *12*, 82–88. [[CrossRef](#)] [[PubMed](#)]
44. Zhou, J.; Qian, H.; Chen, C.-F.; Zhao, J.; Li, G.; Wu, Q.; Luo, H.; Wen, S.; Liu, Z. Optical edge detection based on high-efficiency dielectric metasurface. *Proc. Natl. Acad. Sci. USA* **2019**, *116*, 11137–11140. [[CrossRef](#)] [[PubMed](#)]
45. Zhou, J.; Liu, S.; Qian, H.; Li, Y.; Luo, H.; Wen, S.; Zhou, Z.; Guo, G.; Shi, B.; Liu, Z. Metasurface enabled quantum edge detection. *Sci. Adv.* **2020**, *6*, eabc4385. [[CrossRef](#)] [[PubMed](#)]
46. Zhou, J.; Qian, H.; Zhao, J.; Tang, M.; Wu, Q.; Lei, M.; Luo, H.; Wen, S.; Chen, S.; Liu, Z. Two-dimensional optical spatial differentiation and high-contrast imaging. *Natl. Sci. Rev.* **2021**, *8*, nwa176. [[CrossRef](#)] [[PubMed](#)]
47. Liu, S.; Chen, S.; Wen, S.; Luo, H. Photonic spin Hall effect: Fundamentals and emergent applications. *Opto-Electron. Sci.* **2022**, *1*, 220007. [[CrossRef](#)]
48. He, S.; Wang, R.; Luo, H. Computing metasurfaces for all-optical image processing: A brief review. *Nanophotonics* **2022**, *11*, 1083–1108. [[CrossRef](#)]
49. Karimi, E.; Piccirillo, B.; Marrucci, L.; Santamato, E. Light propagation in a birefringent plate with topological charge. *Opt. Lett.* **2009**, *34*, 1225–1227. [[CrossRef](#)]
50. Shu, W.; Liu, Y.; Ke, Y.; Ling, X.; Liu, Z.; Huang, B.; Luo, H.; Yin, X. Propagation model for vector beams generated by metasurfaces. *Opt. Express* **2016**, *24*, 21177–21189. [[CrossRef](#)]

**Disclaimer/Publisher's Note:** The statements, opinions and data contained in all publications are solely those of the individual author(s) and contributor(s) and not of MDPI and/or the editor(s). MDPI and/or the editor(s) disclaim responsibility for any injury to people or property resulting from any ideas, methods, instructions or products referred to in the content.